

## Antiproton-Proton Cross Sections at 1.0, 1.25, and 2.0 Bev\*

RAFAEL ARMENTEROS,† CHARLES A. COOMBES,‡ BRUCE CORK, GLEN R. LAMBERTSON, AND W. A. WENZEL  
Lawrence Radiation Laboratory, University of California, Berkeley, California

(Received April 29, 1960)

The interaction of 1.0-, 1.25-, and 2.0-Bev antiprotons with protons has been studied with the aid of a  $4\pi$  solid-angle scintillation-counter detector system. The measured total cross sections at the above energies are 100, 89, and 80 mb, respectively. At each energy, the charge-exchange cross section is approximately 5 mb. The total elastic cross sections are 33, 28, and 25 mb, respectively, at the three energies. The angular distribution of elastic scattering has been fitted with a simple optical-model calculation.

### INTRODUCTION

AT antiproton energies of 1 Bev and lower, the antiproton-proton total, inelastic, and elastic-scattering cross sections are considerably larger than the corresponding nucleon-nucleon cross sections.<sup>1-6</sup> It is of interest to discover to what extent this difference persists at higher energies. The present experiment was designed to carry the measurements of the  $\bar{p}$ - $p$  cross sections to the highest energy at which an appreciable yield of antiprotons is expected from the Bevatron. Measurements of the elastic, inelastic, total, and charge-exchange cross sections were made at antiproton energies of 1.0, 1.25, and 2.0 Bev. The method involved the use of scintillation counters arranged to form a  $4\pi$  solid-angle detector similar to that used in two previous antiproton experiments.<sup>3,6</sup>

### I. ANTIPROTON BEAM

The beam channel (Fig. 1) which carried the antiprotons from the Bevatron to the liquid-hydrogen target was similar in design to that described by Coombes *et al.*<sup>3</sup> Negative particles from an internal beryllium target in the Bevatron were focused by an 8-in. quadrupole lens,  $Q_1$ . A horizontal image of the target was formed at the entrance to  $Q_2$ , which defined the momentum width of the beam. A vertical image of the target was formed at the entrance to deflecting magnet  $M$ . At this point a partial separation of antiprotons and fast particles was achieved at the two

lower energies by means of a 40-ft parallel-plate velocity selector made from two of the 20-ft separators described by Coombes *et al.*<sup>3</sup> Besides removing the dispersion of the Bevatron, deflecting magnet  $M$  defined the momentum of the beam. Steering magnet  $C_1$  was adjusted to direct into the channel particles of the desired momentum from one of three internal targets. These targets were located so that for any momentum in the range of interest, particles emitted near the forward direction could be selected. The 4-in. quadrupole system  $Q_3 \cdots Q_7$ , conveyed the beam through a system of defining counters to the liquid-hydrogen target. Deflecting magnet  $C_2$  removed positive particles and off-momentum negative particles formed by interactions earlier in the system. The beam emerging from  $Q_7$  was well collimated. Measured 15 ft beyond  $Q_7$ , the width of the beam, both vertically and horizontally, was about 2 in.

Antiprotons in the beam were identified primarily by time of flight. The pulses from six 4- by 4-in. scin-

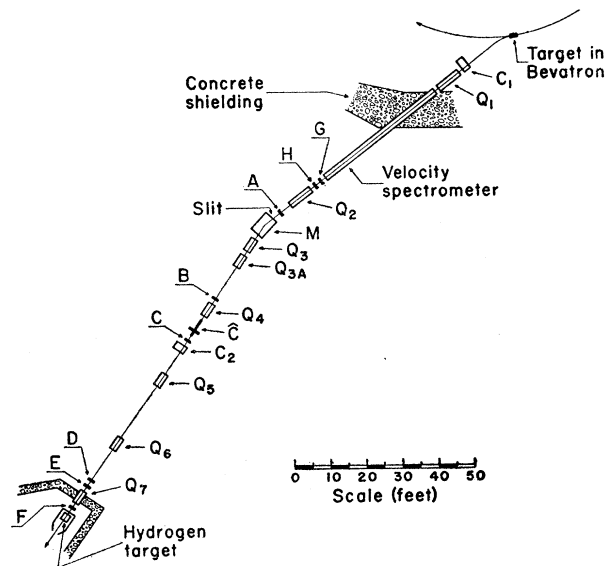


FIG. 1. Experimental arrangement. Here  $C_1$ ,  $C_2$ , and  $M$  are deflecting magnets. Quadrupole sets  $Q_1$  and  $Q_2$  have 8-inch apertures;  $Q_3$ - $Q_7$  have 4-in. apertures. Counters  $A$  through  $F$  are 4- by 4- by  $\frac{1}{4}$ -in. plastic scintillators used for time-of-flight measurement. Counters  $G$  and  $H$  are 4- by 8- by  $\frac{1}{4}$ -in. counters, and  $C$  is a gas Čerenkov counter used to reject pions.

\* This work was done under the auspices of the U. S. Atomic Energy Commission.

† On leave of absence from Conseil Nucléaire de Recherche Scientifique and Laboratoire de Physique, Ecole Polytechnique, Paris, France.

‡ Present address: University of Idaho, Pocatello, Idaho.

<sup>1</sup> Bruce Cork, G. R. Lambertson, O. Piccioni, and W. A. Wenzel, Phys. Rev. **107**, 248 (1957).

<sup>2</sup> O. Chamberlain, D. V. Keller, R. Mermod, E. Segrè, H. M. Steiner, and T. J. Ypsilantis, Phys. Rev. **108**, 1553 (1957).

<sup>3</sup> C. A. Coombes, Bruce Cork, W. Galbraith, G. R. Lambertson, and W. A. Wenzel, Phys. Rev. **112**, 1303 (1958).

<sup>4</sup> G. Goldhaber, T. Kalogeropoulos, and R. Silberberg, Phys. Rev. **110**, 1474 (1958).

<sup>5</sup> L. E. Agnew, T. Elioff, W. B. Fowler, L. J. Gilly, R. L. Lander, L. O. Oswald, W. M. Powell, E. Segrè, H. M. Steiner, H. S. White, C. E. Wiegand, and T. J. Ypsilantis, University of California Radiation Laboratory Report UCRL-8822, June, 1959 (unpublished).

<sup>6</sup> T. Elioff, L. E. Agnew, O. Chamberlain, H. M. Steiner, C. E. Wiegand, and T. J. Ypsilantis, Phys. Rev. Letters **3**, 285 (1959).

tillation counters (*A* through *F* of Fig. 1), mixed in two fast threefold coincidence circuits, were used at the two lower momenta. At 2.0 Bev, two other counters (*G* and *H* in Fig. 1) were added. These were inserted early in the beam channel, and the time-of-flight distance used was increased from 90 to 120 ft. An additional fast coincidence circuit including signals from *G* and *H* increased the discrimination against unwanted particles.

In addition to the time-of-flight system, the pulse from a gas Čerenkov counter (Fig. 2) connected in anticoincidence into each of the fast coincidence circuits was used to reject pions, muons, and electrons. Operated at 180 psi of methane, this counter did not respond to  $K^-$  mesons and antiprotons in the beam. Methane was selected as the Čerenkov radiator because of its relatively large product of index of refraction times radiation length. The loss of particles from absorption and scattering in the 6-ft gas counter was very small.

Separation of antiprotons from background particles was most difficult at the highest energy ( $T_{\bar{p}}=2.0$  Bev). Figure 3 shows the yield at this energy of detected particles in the beam as the tuning of the time-of-flight system was varied. The point marked  $\pi^-$  was obtained without the pulse from the gas counter. It gives the relative number of pions, muons, and electrons in the beam. With the signal from the gas counter in anticoincidence, the detected yield was reduced by a factor of about  $10^4$ . From the symmetry of the delay curve about the time of flight of the  $K^-$  meson, it is probable that most of these particles detected with the tuning set for fast particles are  $K$  mesons. Therefore an upper limit of  $10^{-4}$  can be set on the inefficiency of the gas counter as a detector of fast particles.

From the solid delay curve of Fig. 3 it is not obvious that the  $K$  mesons and antiprotons are cleanly separated. The dashed curves indicate the expected shape of the yield curves for  $K$  mesons and antiprotons, respectively. These curves were determined from the delay curve for fast particles, as measured without the gas Čerenkov counter. A characteristic of this curve is that on a semilog plot, it is convex downward in the

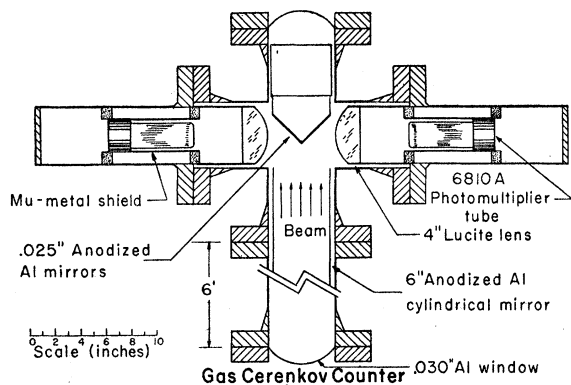


FIG. 2. Diagram of construction of the gas Čerenkov counter.

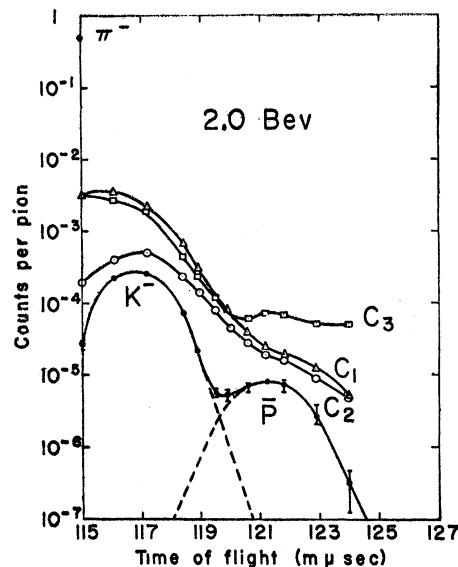


FIG. 3. Delay curve for time-of-flight counters at 2.8 Bev/ $c$ . The curves labeled  $C_1$ ,  $C_2$ , and  $C_3$  are outputs of threefold coincidence circuits. The bottom curve is threefold coincidence between  $C_1$ ,  $C_2$ , and  $C_3$ . The ordinate is normalized to the number of pions in the beam. The abscissa is the cable delay between counters *G* and *F* at 2.8 Bev/ $c$ . The point marked  $\pi^-$  indicates the fraction of pions that were counted when the cable delay was set for pions and the anticoincidence Čerenkov counter input was removed.

absence of background from accidental coincidences. The background due to accidentals is negligible as a result of the high efficiency of the gas counter for rejection of the fast particles in the beam. Therefore, using the dashed curves as a basis, we believe that there is less than 1% contamination of the selected antiprotons. The beam characteristics are given in Table I for each momentum.

## II. EXPERIMENTAL PROCEDURE

The experimental procedure was similar to that described by Coombes *et al.*<sup>3</sup> The liquid-hydrogen target (Fig. 4) was completely surrounded by a sufficient number of scintillation counters to distinguish interactions according to whether they were elastic scatterings, charge exchanges, or inelastic processes. The mul-

TABLE I. Beam characteristics. The momentum bandwidth was  $\pm 6\%$ . All quantities were measured at the exit of the magnet channel and correspond to operation with the velocity separator off. Operation of the separator at 360 kv reduces the flux of fast particles by the factor shown. The measured  $K^-$  yield was corrected for decay in flight, and the values given correspond to production yields at the Bevatron target. The  $\pi^-$  flux was not corrected for decay in flight or for electron contamination.

Average momentum (Bev/ $c$ ) ( $\pm 3\%$ )	Solid angle ( $10^{-3}$ sr)	$\bar{p}/\bar{p}$ ( $10^{-2}$ ) ( $\pm 40\%$ )	$\pi^-/\bar{p}$ ( $10^{-3}$ ) ( $\pm 40\%$ )	$\bar{p}/\pi^-$ ( $10^{-6}$ )	$K^-/\pi^-$ ( $\pm 40\%$ )	Separator rejection factor ( $\pm 30\%$ )
1.7	0.40	60	1.3	$45 \pm 5$	0.028	3
2.0	0.33	60	1.2	$48 \pm 5$	0.015	2
2.8	0.50	15	0.9	$15 \pm 5$	0.009	...

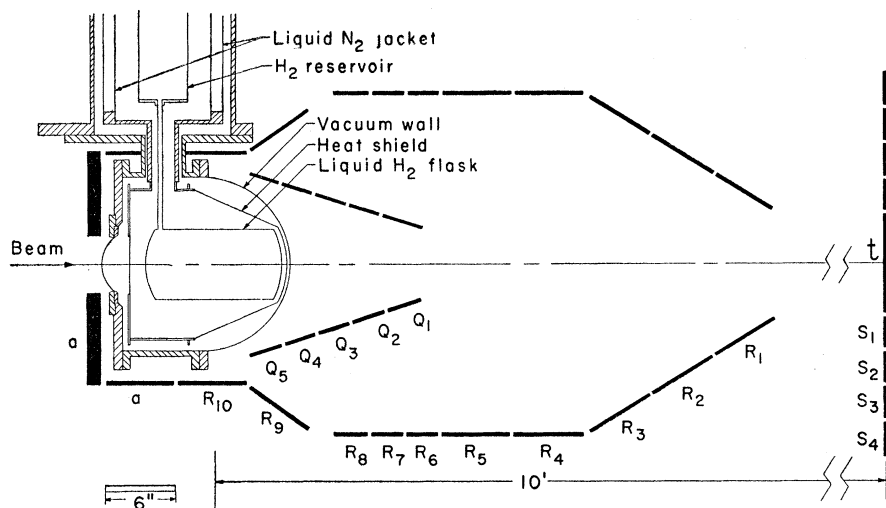


FIG. 4. Liquid-hydrogen target and surrounding counters. The target flask of 0.010-in. stainless steel was surrounded by a 0.003-in. copper heat shield and a 0.040-in. aluminum wall in the forward direction (gasket details are not shown). Counters  $a$ ,  $t$ ,  $Q_1$  through  $Q_5$ ,  $R_1$  through  $R_{10}$ , and  $S_1$  through  $S_4$  were plastic scintillation counters. A  $\frac{1}{4}$ -in. sheet of lead (not shown), between the  $a$  counters and the  $H_2$  target helped in the identification of inelastic events by converting  $\gamma$  rays from  $\pi^0$  decay.

tiplicity of counters was increased considerably over that of the previous experiment to permit measurements at high energies of the elastic-scattering cross section at small angles. The signal from each counter was fed into a multichannel coincidence circuit where it was mixed with a 20  $\mu$ sec gate formed when an antiproton entered the hydrogen target. The gated signals were added along a 125-ohm transmission line, displayed on the trace of a Tektronix-517 oscilloscope, and photographed on 35-mm film. In this way the signal from each of 40 counters was recorded for each antiproton detected. Preliminary classification of events was made as follows:

- (a) A count in the "good geometry" counter,  $t$ , indicated no interaction.
- (b) A count in the backward counters,  $a$ , indicated an inelastic interaction.
- (c) An event in which three or more particles were detected was inelastic.
- (d) If two particles were detected, the event was inelastic or elastic depending upon whether or not the kinematics for an elastic event were satisfied. Use of the  $q$  and  $s$  counters together permitted accurate angular definition at large angles in spite of the length of the hydrogen target.
- (e) No count in any of the  $a$ ,  $q$ ,  $r$ ,  $s$ , or  $t$  counters indicated a charge exchange.

Corrections were made according to the methods outlined by Coombes *et al.* for accidentals, self-absorption in the counters, and counter inefficiencies.<sup>3</sup> Differences between hydrogen in and out permitted background subtraction. Total cross-section measurements were corrected for forward scattering by means of the optical theorem relating the imaginary part of the forward-scattering cross section to the total cross section. The experimental cross sections are given in Table II. Figures 5, 6, and 7 show the measured angular distributions of the elastic scattering at each energy.

The charge-exchange cross section as measured in this experiment was the "elastic" charge-exchange cross section. From the definition given above of the charge-exchange events, it is clear that some contamination of the charge-exchange events could have come from inelastic events, including annihilations into neutral particles. This is true partly because the lead converter surrounding the hydrogen target, which was required for the detection of the  $\gamma$  rays from  $\pi^0$  decay, covered only the back half of the center-of-mass solid angle. The amount of contamination of the charge-exchange cross section due to inelastic processes can be estimated as follows. For  $\bar{p}$ - $p$  interactions, backward-forward symmetry of  $\pi^0$  production follows from invariance under charge conjugation. By comparing the number of (inelastic) events in which only the back counters

TABLE II. Antiproton-proton cross sections. The forward scattering correction has been made with the use of the optical theorem. The indicated errors are both statistical and systematic in origin.

Kinetic energy (Bev)	Total cross section (mb)	Observed elastic cross section (mb)	Minimum cutoff angle (deg c.m.)	Forward-scattering correction (mb)	Corrected elastic cross section (mb)	Charge-exchange cross section (mb)	Inelastic cross section (mb)
1.0 $\pm$ 0.05	100 $\pm$ 3	31 $\pm$ 2	5.4	2	33 $\pm$ 2	5 <sub>-1.5</sub> <sup>+1</sup>	62 $\pm$ 3
1.25 $\pm$ 0.07	89 $\pm$ 4	26 $\pm$ 2	5.7	2	28 $\pm$ 2	4 $\pm$ 1	57 $\pm$ 4
2.00 $\pm$ 0.09	80 $\pm$ 6	22 $\pm$ 4	6.3	3	25 $\pm$ 4	6 <sub>-3</sub> <sup>+2</sup>	49 $\pm$ 6

counted with the number of inelastic events in which only the forward counters counted, we can determine how often the lead converter is required for the detection of an inelastic event. From this we can estimate the probability that an inelastic event was not detected and was classified as a charge exchange. Contamination from this effect amounts to at most a 1-mb error in the cross section. This has been included in the errors given in Table II.

### III. OPTICAL MODEL

An optical model was used to fit the experimental cross sections of Table II and Figs. 5, 6, and 7.<sup>7</sup> The ray model, in which the summation over angular-momentum states is done in integral form, was used. A purely absorptive interaction was assumed. In this case, the elastic and total cross sections, respectively, may be written

$$\sigma_e = 2\pi \int_0^\infty [1 - a(\rho)]^2 \rho d\rho, \quad (1)$$

and

$$\sigma_t = 4\pi \int_0^\infty [1 - a(\rho)] \rho d\rho, \quad (2)$$

where  $\rho$  is the projected distance from the center of the interaction measured on a plane perpendicular to the

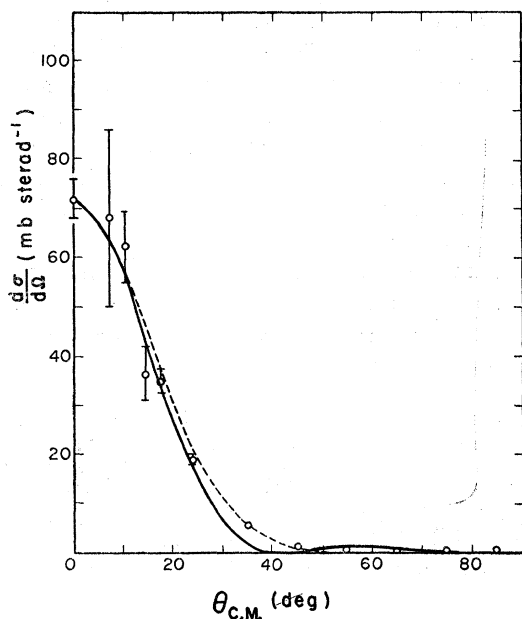


FIG. 5. Angular distribution of elastic scatterings at 1.0 BeV. The zero-degree point was obtained from the measured total cross section with the help of the optical theorem. It is a minimum value, as is predicted for a purely absorptive interaction. The curves are from optical-model calculations described in the text. Indicated uncertainties are statistical only.

<sup>7</sup> S. Fernbach, R. Serber, and C. J. Taylor, Jr., Phys. Rev. 75, 1352 (1949).

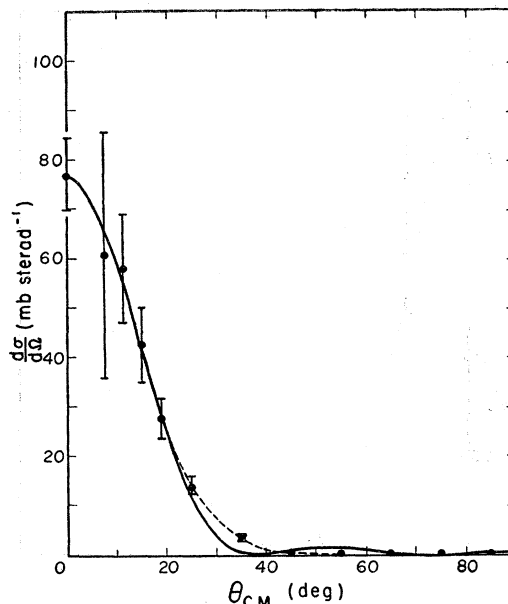


FIG. 6. Angular distribution of elastic scatterings at 1.25 BeV.

direction of initial motion, and  $a(\rho)$  is the amplitude of the antinucleon wave after transmission of the region of interaction. The amplitude for elastic scattering through angle  $\theta$  is given by

$$f(\theta) = k \int_0^\infty [1 - a(\rho)] J_0(2k\rho \sin(\theta/2)) \rho d\rho, \quad (3)$$

where  $k$  is the wave number of the nucleon in the center of mass, and  $J_0$  is the Bessel function of zeroth order. The form of the argument of  $J_0$  is that recommended by Glauber.<sup>8</sup>

Two different models were tried:

(1) *Gray disk*. For this model we have  $a(\rho) = a_0$  for  $\rho < R$  and  $a(\rho) = 1$  for  $\rho > R$ . The results for the gray disk are similar to those for a gray sphere, and calculations are easier.

(2) *Short-range black disk with outside region of decreasing absorption*. For this model we have  $a(\rho) = 0$  for  $\rho < R_0$ , and  $a(\rho) = 1 - \exp[-(\rho^2 - R_0^2)/\rho_0^2]$  for  $\rho > R_0$ . For each model two parameters are determined from Eqs. (1) and (2). At each energy, values found for  $a_0$  and  $R$  in Model 1 and  $R_0$  and  $\rho_0$  in Model 2 are given in Table III. With these values and Eq. (3), angular distributions were calculated. The solid curves of Figs. 5, 6, and 7 are for Model 1; the dashed curves are for Model 2. The experimental results appear to favor the interaction that falls off slowly with the radius over the one in which a sharp boundary exists. At lower energies,<sup>3</sup> on the other hand, it has been shown earlier that the black-sphere approximation gives a good fit to the data. The significance of these results is limited to some

<sup>8</sup> R. J. Glauber, *Lectures in Theoretical Physics* (Interscience Publishers Inc., New York, 1959), p. 345.

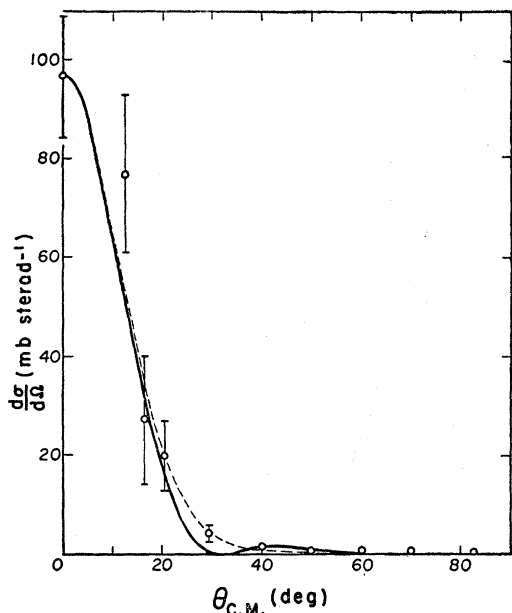


FIG. 7. Angular distribution of elastic scatterings at 2.0 Bev.

extent by approximations and assumptions made in applying the optical model. At low energies, for example, the number of partial waves required to describe the interaction is small.<sup>9</sup>

For the present analysis we have neglected potential scattering. While this probably has little effect on the large forward scattering, it may contribute a significant part of the large-angle scattering. It should be noted that in this experiment we have

$$\left(\frac{d\sigma}{d\Omega}\right)_{\text{measured}} = \frac{d\sigma(\theta)}{d\Omega} + \frac{d\sigma(\pi-\theta)}{d\Omega}, \quad (4)$$

for  $30 \text{ deg} < \theta < 150 \text{ deg}$ . This follows from the kinematic symmetry of the interaction in the center-of-mass system and the fact that the energy is high enough that antiprotons scattered at angles as large as 150 deg may escape from the target.

#### IV. DISCUSSION

In Fig. 8, the experimental  $\bar{p}$ - $p$  total, elastic, and charge-exchange cross sections are plotted, together with the results of other experiments in which the energy dependences of the cross sections were measured. The total  $pp$  and  $np$  cross sections at corresponding energies are shown for comparison. The results of the present experiment are in good agreement with those of Eloff *et al.* for antiproton energies near 1 Bev.<sup>6</sup>

As with the measured nucleon-nucleon interactions, it is expected that the character of the antinucleon-nucleon interaction will change at energies above

<sup>9</sup> J. S. Ball and G. F. Chew, Phys. Rev. **109**, 1395 (1958).

threshold for pion production. For this reason, optical Model 2 is somewhat more appealing than Model 1 because it provides for an interaction region of low opacity and large radius comparable with the Compton wavelength of the pion. It has been shown that such an interaction can account for the observed proton-proton cross sections at high energies,<sup>10,11</sup> provided that it is supplemented by a strong short-range potential interaction whose effect falls off with energy. If Model 2 is used to describe the present experiment, the short-range, strongly absorbing region is presumably to be associated with the annihilation interaction. However, the values of  $R_0$  and  $\rho_0$  in Table III should not be interpreted too literally. The indicated errors are related only to the errors in  $\sigma_t$  and  $\sigma_e$ , and some additional variations can be made without causing serious disagreement with the angular distributions of Figs. 5, 6, and 7.

The inelastic  $\bar{p}$ - $p$  cross section includes annihilation, pion production, and possibly other processes. In this experiment these are not distinguished directly. However, there are kinematical differences that under certain assumptions would allow us to distinguish the annihilation events from other inelastic events. For example, it may be possible to separate to some extent annihilation from inelastic pion production by means of multiplicity. For annihilation, the multiplicity is known to be high. Insofar as only the exterior pion cloud is involved, we might expect that inelastic pion production is similar for the nucleon-nucleon and antinucleon-nucleon interactions. There are, however, differences between the  $pp$  and  $pn$  interactions. For the  $pp$  interaction, which occurs in a pure  $T=1$  state, the cross section for single-pion production rises rapidly above threshold, presumably due to the formation of the  $T=3/2$  isobaric state. For the  $pn$  interaction which occurs half the time in  $T=0$  and half the time in  $T=1$ , the pion-production cross section rises more slowly with energy just above threshold. At 1 Bev, on the other hand, the inelastic  $pn$  cross section is about 21 mb, only slightly less than the inelastic  $p$ - $p$  cross section at the same

TABLE III. Optical-model parameters  $a_0$  and  $R$  are the transmission parameter and radius characteristic of a "black disk" interaction used in the first model described in the text;  $R_0$  and  $\rho_0$  are the radii characteristic of the second model discussed in the text. This consists of an opaque core and a longer range tail of decreasing opacity. The radius at which the opacity ( $=1-a^2$ ) of Model 2 falls to one-half is  $\bar{\rho}$ . The indicated errors are derived only from the errors in the cross-section measurements.

$T^-$ (Bev)	$a_0$	$R$ ( $10^{-13}$ cm)	$R_0$ ( $10^{-13}$ cm)	$\rho_0$ ( $10^{-13}$ cm)	$\bar{\rho}$ ( $10^{-13}$ cm)
1.0	$0.34 \pm 0.03$	$1.55 \pm 0.02$	$0.73 \pm 0.06$	$1.03 \pm 0.03$	$1.42 \pm 0.04$
1.25	$0.37 \pm 0.03$	$1.50 \pm 0.02$	$0.61 \pm 0.08$	$1.02 \pm 0.03$	$1.36 \pm 0.04$
2.00	$0.38 \pm 0.07$	$1.43 \pm 0.04$	$0.57 \pm 0.17$	$0.98 \pm 0.07$	$1.33 \pm 0.09$

<sup>10</sup> Bruce Cork, W. A. Wenzel, and C. W. Causey, Phys. Rev. **107**, 859 (1957).

<sup>11</sup> Gerald E. Brown, Phys. Rev. **111**, 1178 (1958).

energy.<sup>12</sup> Since the  $\bar{p}p$  interaction also occurs in a half-and-half mixture of  $T=0$  and  $T=1$ , we might expect that inelastic pion production is more nearly like  $pn$  than  $pp$ . At 2 Bev, two-pion production predominates strongly in the inelastic  $pn$  interaction.<sup>13</sup> Because of the possibility that two-pion production is important, it is doubtful that an effective separation of annihilation and inelastic pion production can be made in the 1- to 2-Bev energy range on the basis of multiplicity.

In the 400- to 700-Mev range there is disagreement between the results of Cork *et al.*<sup>1</sup> and Elioff *et al.*<sup>6</sup> Taken together with the results of Coombes *et al.*<sup>3</sup> for energies below 400 Mev, the results of reference 6 imply a relatively large cross section for pion production, while the lower total cross section found in reference 1 would indicate very little pion production just above threshold.

### V. CONCLUSIONS

The inelastic, elastic, total, and charge-exchange cross sections fall slowly with energy for antiproton energies up to 2 Bev. At 2 Bev the elastic, inelastic, and total cross sections are still considerably larger than the corresponding nucleon-nucleon cross sections. If it is assumed that the pion-production cross section is the same as for the corresponding nucleon-nucleon interaction at the same energy, then the  $\bar{p}p$  annihilation cross section at 2 Bev is about 25 mb.

At energies below threshold for pion production, the experimental results have been fit very well by the semiphenomenological model of Ball and Chew.<sup>9</sup> Relativistic limitations of the potential formalism restrict the use of the Ball-Chew model to low energies. For the present experiment, the inelastic cross section and the differential elastic-scattering cross section have been fit by an optical-model calculation. A good fit can be obtained by assuming a purely absorptive interaction of range about equal to the pion Compton wavelength and consisting of a totally opaque core of range  $0.6$  to  $0.7 \times 10^{-13}$  cm surrounded by a region of lower opacity.

A theorem due to Pomeranchuk predicts with a few plausible assumptions that the difference between par-

<sup>12</sup> A. P. Batson, B. B. Culwick, J. G. Klepp, and L. Riddiford, *1958 International Conference on High-Energy Physics at CERN*, edited by B. Ferretti (CERN Scientific Information Service, Geneva, 1958), p. 74.

<sup>13</sup> W. B. Fowler, R. P. Shutt, A. M. Thorndike, and W. L. Whittemore, *Phys. Rev.* **95**, 1026 (1954).

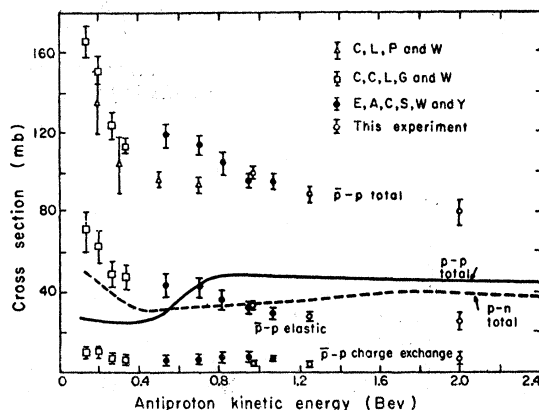


Fig. 8. Energy dependence of total, elastic, and charge-exchange  $\bar{p}p$  cross sections. Results of this experiment are indicated by open circles. The solid circles are from reference 6, open squares from reference 3, and open triangle from reference 1. For comparison,  $p-p$  and  $p-n$  total cross sections are shown. The uncertainties are both statistical and instrumental in origin.

title and antiparticle cross sections vanishes in the high-energy limit.<sup>14</sup> This prediction is in agreement with measurements at Bevatron energies of the charged-pion-nucleon interactions.<sup>15,16</sup> The theorem is obviously not satisfied for the nucleon-nucleon system for energies up to 2 Bev. Because of the greater mass and complexity of the fundamental particles involved, and because the annihilation process plays an important role, it might be expected that cross-section measurements at still higher energies are required to test Pomeranchuk's theorem for the nucleon-nucleon and the antinucleon-nucleon interactions.

### ACKNOWLEDGMENTS

The authors gratefully acknowledge the assistance of C. G. Burton, L. Gilboy, R. L. Crolus, C. L. Wang, R. W. Duncan, M. J. Aiken, and E. J. Rosa in the construction and assembly of the equipment used in the experiment and in the scanning and data-reduction program which followed. We wish also to thank W. Hartsough and the Bevatron crew for their assistance in the setup of the beam channel and for the successful operation of the accelerator during the experiment.

<sup>14</sup> I. Pomeranchuk, *J. Exptl. Theoret. Phys.* **34**, 725 (1958) [translation: *Soviet Phys.-JETP* **34**, 7, 499 (1958)].

<sup>15</sup> Fred Wikner, thesis, University of California Radiation Laboratory Report UCRL-3639, January 10, 1957 (unpublished).

<sup>16</sup> M. Longo, J. Helland, W. Hess, B. J. Moyer, and V. Perez-Mendez, *Phys. Rev. Letters* **3**, 568 (1959).